JOURNAL OF COMPUTATIONAL PHYSICS **136,** 324–336 (1997)
ARTICLE NO. CP975738

Hybrid Simulations of the Effects of Energetic Particles on Low-Frequency MHD Waves

E. V. Belova,*[,1] R. E. Denton,* and A. A. Chan†

*Department of Physics and Astronomy, Dartmouth College, Hanover, New Hampshire 03755; †Rice University, Houston, Texas 77251

Received October 14, 1996; revised April 14, 1997

A hybrid MHD-gyrokinetic simulation model is presented which is suitable for self-consistent study of the interaction of energetic particles with low-frequency MHD waves. Fully electromagnetic gyrokinetic equations are used to describe the energetic particles, while the cold background plasma is treated as a fluid, using nonlinear one-fluid MHD equations. Based on this model a hybrid MHD-gyrokinetic particle code has been developed. A δf algorithm has been implemented in the code for $\beta \sim 1$ electromagnetic perturbations. The gyrokinetic description enables us to remove the restriction on the particle time step dictated by the gyromotion, while the δf algorithm strongly reduces the simulation numerical noise level. Therefore, considerably larger time steps and a smaller number of particles can be used in the simulations as compared to conventional methods. The conservation properties of the model and corresponding δf scheme have been investigated. Representative two-dimensional simulations of the mirror instability and the temperature gradient driven instability of the compressional mode were performed, and the simulation results are in very good agreement with linear theory.

1. INTRODUCTION

The interaction of low-frequency MHD waves with energetic particles is of great interest for space and laboratory plasmas. It arises in any magnetized collisionless plasma system when the plasma can be considered to consist of two components: a low-temperature core plasma and a hot plasma with low density. In particular, the resonant interaction of magnetospheric hydromagnetic waves with high energy protons is one of the leading candidates for explaining Pc 4-5 geomagnetic pulsations [1]; the toroidal Alfvén eigenmode (TAE) driven unstable through resonant interaction with energetic ions may lead to large alpha particle losses in tokamaks [2].

A self-consistent study of the interaction of energetic particles with low-frequency hydromagnetic waves in high-beta (the ratio of plasma to magnetic pressure) magnetized plasma requires nonlinear kinetic calculations. However, conventional particle simulation algorithms are not practical for such study, because of the disparate time scales involved. In particular, in a conventional particle code the time step is determined by the particle gyration, rather than by the mode frequency, and this can be a severe restriction when the time scales of interest are orders of magnitude larger than the cyclotron period. In addition, excessive numerical noise due to the use of a limited number of particles in the simulation of a high beta plasma can also be a problem, especially if the physical instability of interest is a weak resonant type instability with a very low saturation amplitude.

A number of hybrid MHD-gyrokinetic and MHD-drift kinetic models has been developed for analytical and numerical study of kinetic effects on MHD modes with application to the space environment [3], as well as energetic particle effects on MHD stability in tokamaks [4–6]. In these models, energetic particles are treated as gyrokinetic particles, while the cold background plasma is treated as a fluid, using the magnetohydrodynamic description. The gyrokinetic particles are coupled to the fluid equations through their pressure or current [4]. The hybrid approach optimizes the efforts in simulating the two-component system by using the MHD description for the core plasma and employing particle simulations for the energetic component only. The numerical model presented here is similar to the previous hybrid models; however, fully electromagnetic phase-space preserving gyro-center equations [7, 8] are used for energetic particles (ions), the current coupling scheme of Park *et al.* [4] is employed, and a low-noise δf method is implemented for electromagnetic perturbations in a high-beta ($\beta \sim 1$) plasma.

The gyrokinetic equations used in this work were derived from systematic Hamiltonian theory [7, 9, 10] and satisfy both phase volume and energy conservation. The derivation of the gyrokinetic equations is based on the gyrokinetic ordering, which assumes, in particular, that the characteristic frequency of the fluctuations is small compared to the ion gyrofrequency ($\omega \ll \omega_{ci}$) and that the average spatial scale of the perturbation perpendicular to the background magnetic field is comparable to the gyroradius ($k_\perp \rho_h \sim 1$).

[1] E-mail: ebelova@pppl.gov. Present address: Princeton Plasma Physics Laboratory, Princeton University, P.O. Box 451, Princeton, New Jersey 08543.

0021-9991/97 $25.00

The reduced (gyrophase-averaged) system has one less degree of freedom and describes the motion of the gyro-center in the averaged fields. The elimination of the fast particle gyration from the equations of motion allows significant increase of the simulation time step, while the finite Larmor radius effects are retained and, thus, all the relevant physics is kept.

In order to achieve good total energy and particle number conservation in the hybrid MHD-gyrokinetic simulations, the condition $\Delta t < \Delta x_{\|}/v_{th\|}$ has to be satisfied, where v_{th} is thermal velocity, Δx is grid spacing and subscript "$\|$" denotes the direction parallel to the background magnetic field. For typical parameters used in this paper, this condition represents an order of magnitude improvement in particle time step as compared to a hybrid code with kinetic ions, and the time step requirement has to be satisfied for accuracy rather than stability reasons. In the perpendicular direction a grid spacing $\Delta x_{\perp} < \rho_h$ is needed in order to resolve fluctuations with wavelength comparable to the gyroradius.

Even though it was found that the use of gyrokinetic equations for hot particles (instead of following particle trajectories with the Lorentz force equation) greatly reduces the simulation noise level, a very large number of particles is still necessary for 2D or 3D simulation of a weak kinetic type instability. In order to reduce the numerical noise associated with a finite number of simulation particles, we have implemented a low-noise technique called the δf method, in which the perturbation of the distribution function δf, rather than the total distribution function $f = f_0 + \delta f$ is evolved.

In the δf algorithm the zero-order part of distribution function f_0 is assumed to be known analytically, thus the intrinsic noise associated with representation of f_0 by the limited number of simulation particles is totally eliminated. The evolution of δf is calculated along a set of charateristics of the gyro-averaged Vlasov equation. The simulation particles in this case represent points (markers) in phase-space at which the value of the distribution function is known, rather than physical particles, and a time-varying weight $w \sim \delta f/f$ is assigned to each marker particle. According to the estimates [11, 12] the noise intensity in the δf simulations scales as $|\delta f/f|^2$. Thus, the δf algorithm gives a tremendous noise reduction when low amplitude perturbations are considered.

The paper is organized as follows. The hybrid MHD-gyrokinetic model is described in Section 2. In Section 3 the gyro-center equations are presented. The δf method is considered in Section 4. The conservation properties of the hybrid MHD-gyrokinetic δf code are discussed in Section 5. To verify the hybrid MHD-gyrokinetic model, a dispersion relation decribing the coupling of the shear Alfvén wave to the fast magnetosonic mode is derived and compared with the kinetic theory results in Section 6. Two-dimensional simulations of magnetic Landau damping of the compressional mode in a uniform, isotropic plasma and simulations of the mirror instability with temperature ratio $T_{\perp}/T_{\|} = 2.25$ and $\beta_{\|} = 1$ were performed. The drift instability of a compressional mode for $\beta = 0.5$ was also simulated. The simulation results are presented in Section 7. A summary and conclusions are given in Section 8.

2. HYBRID MHD-GYROKINETIC SIMULATION MODEL

We will consider low-frequency (compared to the ion cyclotron frequency) perturbations in a plasma consisting of low temperature isotropic and hot anisotropic components with density $n_h \ll n_b$ and temperature $T_h \gg T_b$. Here subscript "h" denotes the hot ions and subscript "b" (bulk) is used for the rest of the plasma (cold electrons and cold ions). In order to include perpendicular wavelengths with $k_{\perp}\rho_h \sim 1$, the gyro-center equations of motion discussed in Section 3 are used to advance energetic ions, while the dynamics of the bulk plasma is described by nonlinear, compressional, one-fluid MHD equations.

Three-dimensional MHD-gyrokinetic simulations were first used by Park *et al.* [4] to study nonlinear energetic particle effects in tokamaks. Two sets of equations, the pressure coupling and the current coupling scheme, were derived. In the pressure coupling scheme the off-diagonal elements of the hot ion pressure tensor are usually neglected, whereas the current coupling scheme avoids this assumption. In addition, the calculation of the first velocity moment has an advantage over the pressure moment calculation in terms of the numerical noise level. For these reasons the current coupling scheme is used in our model, and the hot ions are coupled to the fluid equations through their current, which appears in the bulk plasma momentum equation [4],

$$\rho_b \frac{d\mathbf{v}_b}{dt} = -\nabla p_b + (\mathbf{j} - \mathbf{j}_h) \times \mathbf{B}/c - en_h\mathbf{E}, \qquad (1)$$

where ρ_b, $\mathbf{v}_b$, and p_b are the bulk plasma density, velocity, and pressure; $\mathbf{j}_h$ is the hot ion current density; $\mathbf{j}$ is total current density; $\mathbf{B}$ and $\mathbf{E}$ are magnetic and electric fields. Note that the second term on the RHS of (1) is the ampere force acting on the bulk component and the third term represents the electric force acting on the excess electrons in the bulk plasma (quasineutrality is assumed).

Other equations for the bulk plasma are the MHD equations

$$\mathbf{E} = -\mathbf{v}_b \times \mathbf{B}/c \qquad (2)$$

$$\mathbf{B} = \mathbf{B}_0 + \nabla \times \mathbf{A} \qquad (3)$$

$$\partial \mathbf{A}/\partial t = -c\mathbf{E} \qquad (4)$$

$$\mathbf{j} = \frac{c}{4\pi}\nabla \times \mathbf{B} \tag{5}$$

$$\partial p_b^{1/\gamma}/\partial t + \nabla \cdot (\mathbf{v}_b p_b^{1/\gamma}) = 0 \tag{6}$$

$$\partial \rho_b/\partial t + \nabla \cdot (\mathbf{v}_b \rho_b) = 0. \tag{7}$$

Here $\mathbf{B}_0$ is the equilibrium magnetic field, $\mathbf{A}$ is a modified vector potential (different from the usual vector potential by a term involving the gradient of the scalar potential), and an adiabatic equation of state is used. We assume that the hydromagnetic approach for disturbances is justified by the presence of the dense cold population, which allows the neglect of parallel electric fields. The validity of this assumption was discussed, for example, by Southwood [13] and Cheng [3].

3. GYROKINETIC EQUATIONS

In this section the equation of motion used to advance the energetic ions in the simulation and the calculation of the hot ion density and current are described. Since we want to include the hot ion kinetic effects such as finite Larmor radius and wave-particle resonances, the low-frequency gyrokinetic equations are employed to describe the hot particle dynamics. The use of electromagnetic gyrokinetic equations with spatial gyroaveraging [14] allows us to eliminate the fast gyromotion time scale and consider perturbations with perpendicular wavelength comparable to the hot ion gyroradius.

The gyrokinetic ordering, which assumes that

$$\frac{\omega}{\omega_{ci}} \sim \frac{\rho_h}{L} \sim \frac{k_\parallel}{k_\perp} \sim \frac{e\varphi}{T} \sim \frac{\delta B}{B} = O(\varepsilon), \quad k_\perp \rho_h = O(1) \tag{8}$$

is adopted in this paper. Here ρ_h is the gyroradius, L is the equilibrium scale length, $k_\parallel$ and $k_\perp$ are the parallel and perpendicular wave numbers, δB and φ are the perturbation of magnetic field and electrostatic potential, and $\varepsilon \ll 1$ is the smallness parameter.

The gyrokinetic equations, derived from a systematic Hamiltonian theory [7, 9, 10], were used in the simulation code. Their derivation is based on the Lie perturbation method [15], which allows one to systematically remove gyro-angle dependence from the system to any desired order, providing a transformation from physical space coordinates ($\mathbf{x}$, $\mathbf{v}$) to gyro-center coordinates ($\mathbf{X}$, U, μ, θ), where $\mathbf{X}$ is the gyrocenter position, U is the parallel velocity, μ is the first adiabatic invariant, and θ is the gyro-angle. Note that the values of $\mathbf{X}$, U, and μ in the transformed space differ from those in physical space by small terms $O(\varepsilon)$; in particular $U = v_\parallel + O(\varepsilon)$ and $\mu = v_\perp^2/2B_0 + O(\varepsilon)$. The main advantage of this formalism is that it preserves the Hamiltonian symmetry of the original Vlasov–Maxwell system and, consequently, the resulting equations are phase-space preserving and allow the construction of an energy integral, which is desirable for numerical purposes.

The equations, which were derived using the action-variational method [7, 8], are

$$\dot{\mathbf{X}} = \frac{1}{B_\parallel^{**}}[\mathbf{B}^{**}U - \hat{\mathbf{b}} \times (\langle \mathbf{E} \rangle - \mu \nabla B_0 + \nabla \langle \mathbf{v}_\perp \cdot \mathbf{A} \rangle)], \tag{9}$$

$$\dot{U} = \frac{\mathbf{B}^{**}}{B_\parallel^{**}} \cdot (\langle \mathbf{E} \rangle - \mu \nabla B_0 + \nabla \langle \mathbf{v}_\perp \cdot \mathbf{A} \rangle), \tag{10}$$

$$\dot{\mu} = 0, \tag{11}$$

where $\mathbf{B}^{**} = \mathbf{B}_0 + \langle \delta \mathbf{B} \rangle$, $B_\parallel^{**} = B_0 + \langle \delta B_\parallel \rangle$, $\delta \mathbf{B} = \nabla \times \mathbf{A}$; $\hat{\mathbf{b}}$ is the unit vector along the equilibrium magnetic field; $\mathbf{v}_\perp$ is particle perpendicular velocity; $\langle\ \rangle \equiv \oint d\theta/2\pi$ and units in which $e = m = c = 1$ are used. In Eqs. (9) and (10) $B_0 = B_0(\mathbf{X})$ is the value of the equilibrium magnetic field at the gyro-center position, while all the perturbed fields are taken at the particle position $\mathbf{x} = \mathbf{X} + \boldsymbol{\rho}_h$, where $\boldsymbol{\rho}_h$ is gyroradius vector. These equations are first-order accurate in the perturbation field amplitude and contain high order terms, which ensure the Hamiltonian properties of the system. The particle magnetic moment μ is an invariant of motion and may be treated as a constant parameter in the simulations.

Since there is freedom in choosing the averaging transformation, different equations of motion (in different gyrocenter coordinates) can be derived [7, 10]. The transformation that gives Eqs. (9) and (10) seems to be the most suitable for the hybrid model, because the scalar potential does not appear explicitly in the equations of motion, and the vector potential in the term $\langle \mathbf{v}_\perp \cdot \mathbf{A} \rangle$ can be calculated easily from (4), without the usual $\nabla\varphi$ term, after one notes that $\langle \mathbf{v}_\perp \cdot \nabla\varphi \rangle = B_0 \langle \partial\varphi/\partial\theta \rangle = 0$. Thus, there is no need to solve for φ, and a simple explicit time stepping scheme can be used to advance the fields using Eqs. (1)–(7) and then use the calculated field values to push the particles. In fact, Eqs. (9) and (10) can be written in a form which does not involve the vector potential at all, because to first order in the smallness parameter ε the following relation holds: $\nabla \langle \mathbf{v}_\perp \cdot \mathbf{A} \rangle = \langle \mathbf{v}_\perp \times \delta \mathbf{B} \rangle$. This form does not conserve energy exactly, but it can have better numerical properties with respect to short wavelength perturbations.

In our hybrid MHD-gyrokinetic code we are using the energy conserving form of Eqs. (9) and (10), which are advanced in time using the leap-frog trapezoidal scheme. Following the numerical procedure described by Lee [14], the gyroaverages are calculated using either four or eight point spatial averaging along the gyro-orbit. The term $\nabla \langle \mathbf{v}_\perp \cdot \mathbf{A} \rangle$ is calculated at the particle location by analytical differentiation of the interpolation function.

The gyro-center particles are described in terms of the gyro-center distribution function $F(\mathbf{X}, U, \mu)$, so that transformation of the zero and first velocity moments is required to calculate the hot ion density and current density in physical space:

$$n_h(\mathbf{x}) = \int \delta(\mathbf{X} + \boldsymbol{\rho}_h - \mathbf{x}) F(\mathbf{X}, U, \mu) d^3\mathbf{X}\, dU\, d\mu\, d\theta \tag{12}$$

$$\mathbf{j}_h(\mathbf{x}) = \int (\dot{\mathbf{X}} + \mathbf{v}_\perp) \delta(\mathbf{X} + \boldsymbol{\rho}_h - \mathbf{x}) F(\mathbf{X}, U, \mu) d^3\mathbf{X}\, dU\, d\mu\, d\theta. \tag{13}$$

In the code this is done by distributing each gyrokinetic particle as four or eight subparticles uniformly around the gyro-orbit with the center at $\mathbf{X}$ and radius ρ_h, and summing up the contributions from all subparticles when calculating current and density [14]. The resulting n_h and $\mathbf{j}_h$ are then substituted into the bulk momentum equation (1). Spatial gyroaveraging in Eqs. (9), (10) and the transformation to physical space in (12) and (13) are done in the same way, and this procedure resolves finite Larmor radius effects for $k_\perp \rho_h = O(1)$. Linear spline interpolation is used to accumulate n_h and $\mathbf{j}_h$, as well as for calculation of the particle drift velocity (9) and parallel acceleration (10).

Equations (1)–(13) constitute a hybrid MHD-gyrokinetic model for describing low-frequency MHD type phenomena in cases where the parallel electric field effects can be neglected. Ohm's law (2) assumes also that $n_h \ll n_b$, so that the electric field is determined by the bulk plasma motion only, rather than by the dynamics of the whole plasma. Since the polarization drift is not included in the expression for the hot ion current (13), the hot ion perpendicular inertia is neglected, compared to the bulk plasma perpendicular inertia in the momentum equation (1) as well.

The dispersion analysis of the hybrid MHD-gyrokinetic equations (1)–(13) presented in Section 6 shows that the model correctly describes compressional type perturbations, provided that ordering (8) holds. The transverse Alfvén waves are accurately described by the model if the conditions $\omega \ll k_\parallel v_{th\parallel}$ and $\omega \ll \omega^*$ are satisfied, where ω^* is the drift frequency. Thus the model can be used to study the interaction of shear Alfvén waves with energetic ions when the particle energy is high enough, so that the drift velocity is large compared to the phase speed of the wave. In particular, the model can be applied to the study of the interaction of low-frequency MHD waves observed in the dayside magnetosphere [16, 17] with energetic (100–200 keV) ring current ions, because the frequency associated with the ion bounce motion along magnetic field lines and ion magnetic drift frequency are large compared to the frequency of the wave. When perpendicular hot ion inertia effects are important, expression (13) has to be modified to include the ion polarization current, and the whole plasma fluid velocity should appear in Ohm's law (2).

4. δf METHOD

In the δf method the zero-order distribution function is assumed to be known, so the zero-order density n_{h0} and current $\mathbf{j}_{h0}$ can be calculated analytically. The perturbed part of the distribution function is calculated along a set of characteristics (9)–(11) by assigning a weight $w \sim \delta f$ to each simulation particle. The particle weights are then used to calculate the perturbed hot ion density δn_h and current density $\boldsymbol{\delta}\mathbf{j}_h$. Since the particle weight is no longer a constant of the motion (as in the conventional particle simulation method), the evolution equation for the weight has to be added to the equations of motion (9) and (10). We will derive the evolution equation for the weight from the Vlasov equation using a definition of weight which is analogous to that of Parker and Lee [18].

We will start by writing the equation for the gyro-center distribution function $F(\mathbf{X}, U, \mu, t)$, assuming that F includes the Jacobian of the transformation from physical-space coordinates to gyro-center coordinates following Littlejohn [15], that is,

$$F = B_\parallel^{**} f(\mathbf{X}, U, \mu, t), \tag{14}$$

where $J = B_\parallel^{**}$ is the Jacobian and $f(\mathbf{X}, U, \mu, t)$ is the particle distribution function expressed in gyro-center coordinates. The number of particles in a phase-space volume element $d\Gamma = B_\parallel^{**}\, d\mathbf{Z}$ is equal to $dN = F\, d\mathbf{Z} = f\, d\Gamma$, where $\mathbf{Z} = (\mathbf{X}, U, \mu)$. The conservation of particles then implies [15, 19]:

$$\frac{\partial}{\partial t} F + \frac{\partial}{\partial \mathbf{X}} \cdot (\dot{\mathbf{X}} F) + \frac{\partial}{\partial U} (\dot{U} F) = 0. \tag{15}$$

Since the equations of motion (9)–(11) preserve phase-space volume $d\Gamma$, the Liouville theorem holds,

$$\frac{\partial}{\partial t} B_\parallel^{**} + \frac{\partial}{\partial \mathbf{X}} \cdot (\dot{\mathbf{X}} B_\parallel^{**}) + \frac{\partial}{\partial U} (\dot{U} B_\parallel^{**}) = 0, \tag{16}$$

which can be proved directly by using Eqs. (9) and (10). As can be seen from (15) and (16), f satisfies the Vlasov equation in gyro-center coordinates, that is,

$$\frac{df}{dt} = \frac{\partial f}{\partial t} + \dot{\mathbf{X}} \cdot \frac{\partial f}{\partial \mathbf{X}} + \dot{U} \frac{\partial f}{\partial U} = 0. \tag{17}$$

The moments of F in the simulations are calculated using a limited number of points in phase-space at which the value of F is known. The positions of these points corre-

spond to the positions of the simulation particles which are regarded as Lagrangian markers [12, 20, 21]. We will distinguish between the physical particles described by the distribution function F and the simulation (marker) particles which are described by a discrete distribution function $\hat{P}(\mathbf{Z}, t)$. The marker distribution can be written in the Klimontovich representation as

$$\hat{P}(\mathbf{Z}, t) = \sum_{m=1}^{M} \delta(\mathbf{X} - \mathbf{X}_m)\delta(U - U_m)\delta(\mu - \mu_m), \quad (18)$$

where m is the marker index and M is the total number of marker particles in the simulation. As was pointed out by Lee [14], particle pushing is equivalent to solving the equation

$$\frac{\partial}{\partial t}\hat{P} + \frac{\partial}{\partial \mathbf{Z}} \cdot (\dot{\mathbf{Z}}\hat{P}) = 0, \quad (19)$$

which has the same form as Eq. (15) for F. Note that, as follows from (16),

$$\frac{\partial \dot{\mathbf{Z}}}{\partial \mathbf{Z}} = \frac{\partial \dot{\mathbf{X}}}{\partial \mathbf{X}} + \frac{\partial \dot{U}}{\partial U} = \frac{1}{B_\parallel^{**}} \frac{dB_\parallel^{**}}{dt} \neq 0; \quad (20)$$

thus the particle motion in the gyro-center space ($\mathbf{X}$, U, μ) described by (9)–(11) is compressible, so Eqs. (15) and (16) cannot be reduced to the usual form of the Vlasov equation (17).

We can define the smooth marker distribution function $P(\mathbf{Z}, t)$ as an ensemble average of $\hat{P}$, and then define particle weight as

$$w = \frac{B_\parallel^{**}\delta f}{P}, \quad (21)$$

where $\delta f = f - f_0$. If P is chosen such that $P(\mathbf{Z}, t) = F(\mathbf{Z}, t)$, then from (14) we have

$$B_\parallel^{**} f_0 = (1 - w)P, \quad (22)$$

and the following time evolution equations for w can be obtained using Eqs. (15) and (17):

$$\dot{w} = -(1 - w)\frac{1}{f_0}\frac{df_0}{dt}. \quad (23)$$

Our definition of the weight is different from that of Hu and Krommes [12], where the general case of compressible particle dynamics was considered and marker weight was defined as $w = \delta F/P$. The definition of w in (21) results in a simpler evolution equation, because the term involving the divergence of the phase-space velocity $\partial\dot{\mathbf{Z}}/\partial\mathbf{Z}$ does not appear on the RHS of Eq. (23) as it does in [12]. Extra calculations are needed, however, to express δF in terms of w and the marker distribution function P. Upon recalling $B_\parallel^{**} = B_0 + \langle \delta B_\parallel \rangle$ we have $\delta F = B_\parallel^{**} f - B_0 f_0 = B_\parallel^{**}\delta f + \langle \delta B_\parallel \rangle f_0$, so that $\delta F = (w + (1 - w)\langle \delta B_\parallel \rangle / B_\parallel^{**})P$. Thus, in the simulations δF can be approximated by the weighted Klimontovich distribution as

$$\delta F \approx \sum_{m=1}^{M} d_m \delta(\boldsymbol{X} - \boldsymbol{X}_m)\delta(U - U_m)\delta(\mu - \mu_m), \quad (24)$$

where we have defined

$$d_m = w_m + (1 - w_m)\left.\frac{\langle \delta B_\parallel \rangle}{B_\parallel^{**}}\right|_{\mathbf{Z}=\mathbf{Z}_m}. \quad (25)$$

Now consider the calculation of a phase-space integral of the general form

$$I(A) = \int A(\mathbf{Z}, t)F(\mathbf{Z}, t)\, d\mathbf{Z}. \quad (26)$$

Separating the zero-order part and the perturbation, we can rewrite the integral for $I(A)$ as

$$I(A) = \int A_0 F_0\, d\mathbf{Z} + \int [A_0\, \delta F + \delta A F]\, d\mathbf{Z}, \quad (27)$$

where $A = A_0 + \delta A$ and $F = F_0 + \delta F$.

The first integral in (27) is assumed to be calculated analytically, while the particle simulations are applied to the calculation of the second integral. To find an estimate for it we let $F \approx \hat{P}$ and use the approximation (24) for δF. Then (27) becomes

$$I(A) = \int A_0 F_0\, d\mathbf{Z} + \sum_{m=1}^{M} [A_0 d_m + \delta A]|_{\mathbf{Z}=\mathbf{Z}_m}. \quad (28)$$

In particular, to calculate particle density (12), we let $A_0 = \langle \delta(\mathbf{X} + \boldsymbol{\rho}_h - \mathbf{x}) \rangle$ and $\delta A = 0$, so that

$$n_h(\mathbf{x}) = n_{h0}(\mathbf{x}) + \sum_{m=1}^{M} d_m \langle \delta(\mathbf{X}_m + \boldsymbol{\rho}_m - \mathbf{x}) \rangle. \quad (29)$$

The current (13) can be calculated by choosing $A_0 = \langle (\dot{\mathbf{X}}_0 + \mathbf{V}_\perp)\delta(\mathbf{X} + \boldsymbol{\rho}_h - \mathbf{x}) \rangle$ and $\delta A = \boldsymbol{\delta}\dot{\mathbf{X}} \langle \delta(\mathbf{X} + \boldsymbol{\rho}_h - \mathbf{x}) \rangle$ in (28) to obtain

$$\mathbf{j}_h(\mathbf{x}) = \mathbf{j}_{h0}(\mathbf{x}) + \sum_{m=1}^{M} \langle [(\dot{\mathbf{X}}_{0m} + \mathbf{V}_{\perp m})d_m + \boldsymbol{\delta}\dot{\mathbf{X}}_m]\delta(\mathbf{X}_m + \boldsymbol{\rho}_m - \mathbf{x}) \rangle, \quad (30)$$

where $\dot{\mathbf{X}}_0$ is the zero-order particle drift and $\boldsymbol{\delta}\dot{\mathbf{X}} = \dot{\mathbf{X}} - \dot{\mathbf{X}}_0$.

Assuming that gyroaverages are calculated by distributing the particle charge at N_g points on the ring $|\mathbf{x} - \mathbf{X}_m| = \rho_m$, we can rewrite (29) and (30) as

$$n_h(\mathbf{x}) = n_{h0}(\mathbf{x}) + \sum_{m=1}^{M} \frac{1}{N_g} \sum_{s=1}^{N_g} d_m \delta(\mathbf{X}_m + \boldsymbol{\rho}_{m,s} - \mathbf{x}), \quad (31)$$

$$\mathbf{j}_h(\mathbf{x}) = \mathbf{j}_{h0}(\mathbf{x}) + \sum_{m=1}^{M} \frac{1}{N_g} \sum_{s=1}^{N_g} [(\dot{\mathbf{X}}_{0m} + \mathbf{V}_{\perp m,s}) d_m + \boldsymbol{\delta}\dot{\mathbf{X}}_m] \delta(\mathbf{X}_m + \boldsymbol{\rho}_{m,s} - \mathbf{x}), \quad (32)$$

where index s denotes the sth point on the ring. Equations (31) and (32) were used in the code for calculation of the perturbed hot ion density and current.

5. CONSERVATION LAWS

The conservation properties of particle number, momentum, and total energy of the δf method for the electrostatic slab case were considered by Parker and Lee [18].

Here we consider the conservation of particle number, total parallel momentum, and total energy for the hybrid MHD-gyrokinetic system (1)–(13) when the periodic boundary conditions are applied, and discuss the associated conservation properties of the δf scheme. For the total number of physical particles we have

$$N(t) = \int F(\mathbf{Z}, t)\, d\mathbf{Z}, \quad (33)$$

and Eq. (15) guarantees that the number of particles is conserved: $dN/dt = 0$. Momentum conservation can be derived by integrating Eq. (1) over the simulation volume, using the particle equations of motion (9) and (10) to obtain

$$\frac{d}{dt}\left(\int \rho_b \mathbf{v}_b\, d^3\mathbf{x} + \int U \hat{\mathbf{b}} F\, d\mathbf{Z} \right) = 0, \quad (34)$$

where the second integral in the brackets is the hot ion parallel momentum. Thus, the total parallel momentum of the MHD-gyrokinetic system is conserved in our model. In the perpendicular direction the momentum of the bulk component only appears in Eq. (34), because the hot ion perpendicular inertia has been neglected, compared to that of the bulk plasma in Eqs. (2) and (13).

We will define the hot ion kinetic energy integral as

$$K_h = \int (U^2/2 + \mu B_0 - \langle \mathbf{v}_\perp \cdot \mathbf{A} \rangle) F(\mathbf{X}, U, \mu) d^3\mathbf{X}\, dU\, d\mu. \quad (35)$$

It has the property that the equality $dK_h/dt = \int \mathbf{j}_h \cdot \mathbf{E} d^3\mathbf{x}$ is exact, resulting in exact total energy conservation for the MHD-gyrokinetic system: $dK_h/dt + dE_{\mathrm{MHD}}/dt = 0$, where $E_{\mathrm{MHD}} = \int (\rho_b v_b^2/2 + p_b/(\gamma - 1) + B^2/8\pi) d^3\mathbf{x}$ is the MHD energy.

The diagnostics based on the above conservation laws were implemented in the code and have proven to be useful for an accuracy check and for debugging the code. In the standard "full f" code the total energy is conserved exactly (in the limit $\Delta t \to 0$), the parallel momentum is conserved to the next order in the gyrokinetic smallness parameter ε and particle conservation is trivial. A result of separating the moments of the distribution function into an analytically calculated zero-order part and a numerically evaluated perturbed part is that the number of particles and total energy in the δf algorithm are no longer exactly conserved. However, these conservation laws are maintained in the simulations in the limit of a large number of marker particles and sufficient spatial resolution.

To obtain an estimate for the total number of physical particles in the δf method, we let $A_0 = 1$ and $\delta A = 0$ in Eq. (28), to find $N(t) = N_0 + \sum_{m=1}^{M} d_m$. Assuming that the perturbation amplitude is small at $t = 0$ and that $w(0) = 0$, the particle conservation can be written in the form

$$\delta N = \sum_{m=1}^{M} d_m = 0, \quad (36)$$

which is the same as the result obtained by Hu and Krommes [12], because Eq. (24) implies that one can define weight d also as $d = \delta F/P$, which is their definition of the marker weight.

An estimate for the particle parallel momentum can be obtained from Eq. (28) in the same way, thus $\int UF\, d\mathbf{Z} \approx \sum_{m=1}^{M} U_m d_m$, where we have assumed that the zero-order term vanishes. The parallel momentum conservation equation (34) becomes

$$\int \rho_b v_{b\parallel}\, d^3\mathbf{x} + \sum_{m=1}^{M} U_m d_m = 0, \quad (37)$$

provided that the bulk plasma parallel momentum is zero initially.

For the particle kinetic energy integral (35) one can write

$$K_h = K_{h0} + \sum_{m=1}^{M} [(U_m^2/2 + \mu_m B_0) d_m - \langle \mathbf{v}_\perp \cdot \mathbf{A} \rangle_m]. \quad (38)$$

A number of test runs were performed with K_h calculated as in Eq. (38). It was found that, even though the total energy was conserved when the perturbation amplitude was above the thermal noise level ("full f" noise level), for perturbations with much smaller amplitude the fluctuations of the hot particle kinetic energy were higher than

the wave energy, that is, K_h was "too noisy" and the total energy was not conserved. As a result, a considerably larger number of simulation particles was required to obtain good energy conservation, while very good agreement with linear theory and convergence in the nonlinear behavior could be achieved with a relatively small number of particles. A similar problem was reported by Parker and Lee [18], where one-dimensional gyrokinetic simulations of the electrostatic drift wave instability were performed.

Such large errors for particle kinetic energy can be understood if one estimates how K_h changes at one time step:

$$\Delta K_h = \Delta t \int (\mathbf{j}_{h0} \cdot \mathbf{E})\, d^3\mathbf{x} + \Delta t \int (\boldsymbol{\delta}\mathbf{j}_h \cdot \mathbf{E})\, d^3\mathbf{x}. \quad (39)$$

Although the first term in Eq. (39) is zero analytically (when $\mathbf{j}_{h0} = 0$), or vanishes in the first order in the perturbation amplitude ($\mathbf{j}_{h0} = \text{const}$), the errors in the kinetic energy associated with it do not vanish in the simulations. The associated noise is actually "full f" noise, since it comes from $\mathbf{j}_{h0}$ and can be estimated as $O(\varepsilon)/\sqrt{M}$. When the number of markers M is not large enough, the errors from the first term in Eq. (39) become larger than the second term $\sim O(\varepsilon^2)$ and the total energy is not conserved.

In other words, even though in the δf scheme the noise associated with n_{h0} and $\mathbf{j}_{h0}$ is eliminated from Eq. (1), the particles are moved with drift velocity (9), which includes the zero-order drift, and this unperturbed particle motion in a wave field results in large fluctuations in the particle kinetic energy. We were able to eliminate this noise by calculating

$$\int (\mathbf{j}_{h0} \cdot \mathbf{E})\, d^3\mathbf{x} = \sum_m [\dot{\mathbf{X}}_{m0} \cdot \langle \mathbf{E} \rangle_m + \langle \mathbf{v}_\perp \cdot \mathbf{E} \rangle_m](1 - d_m) \quad (40)$$

at each time step and integrating it in time. Then, instead of K_h we calculate $\delta K_h = K_h - \int\int (\mathbf{j}_{h0} \cdot \mathbf{E})\, d^3\mathbf{x}\, dt$, so that

$$\frac{d}{dt}\delta K_h = \int (\boldsymbol{\delta}\mathbf{j}_h \cdot \mathbf{E})\, d^3\mathbf{x}. \quad (41)$$

As a result, it was possible to obtain good energy conservation even in runs with a very low perturbation amplitude without increasing the number of particles in the simulation. The above discussion indicates that there seems to be a significant numerical noise associated with calculation of second velocity moments. With the current coupling scheme, this issue is merely diagnostic, whereas with the pressure coupling scheme second moment quantities appear in the momentum equation, which can make the current coupling scheme preferable over the pressure coupling scheme.

6. LOCAL DISPERSION RELATION

In this section we derive the local dispersion relation for the linearized hybrid MHD-gyrokinetic system in slab geometry. For simplicity we assume that $T_b = 0$, so that bulk plasma pressure can be neglected in the momentum equation (1). The dispersion relation then describes the coupling between the transverse Alfvén type and compressional (fast magnetosonic) type waves due to the finite hot ion pressure gradient and finite Larmor radius.

The background magnetic field and hot ion pressure gradients are related by the pressure balance condition

$$\frac{B_0}{4\pi}\nabla B_0 + T_\perp \nabla n_{h0} + n_{h0}\nabla T_\perp = 0, \quad (42)$$

where n_{h0} and $T_\perp$ are the zero-order hot ion density and perpendicular temperature, and all the gradients are perpendicular to the equilibrium magnetic field. The zero-order particle distribution function in gyro-center space is taken to be

$$F_0 = n_{h0}(\mathbf{X})\frac{1}{\overline{\mu}} e^{-\mu/\overline{\mu}} f_M(U), \quad (43)$$

where $\overline{\mu}$ is the average magnetic moment, and $f_M(U) = 1/\sqrt{2\pi T_\parallel}\, \exp(-U^2/2T_\parallel)$, a Maxwell distribution function with parallel temperature $T_\parallel$. The particle distribution in physical space corresponding to F_0 is a local Maxwell distribution with nonuniform density and perpendicular temperature, where $\nabla T_\perp/T_\perp = \nabla B_0/B_0$, since $T_\perp(\mathbf{x}) = \overline{\mu} B_0(\mathbf{x})$. For this distribution the equilibrium condition becomes

$$\kappa_n = -\kappa_B(1 + 2/\beta_\perp), \quad (44)$$

where we define $\kappa_n = d \ln n_{h0}/dx$, $\kappa_B = d \ln B_0/dx$ and $\beta_\perp = n_{h0}T_\perp/(B_0^2/8\pi)$.

In agreement with ordering (8), we assume that the local approximation $k_\perp L \gg 1$ is valid, so that the background and perturbation scale lengths in the Vlasov equation (17) are completely separated. In this case, one obtains from Eqs. (16) and (17)

$$\frac{\partial}{\partial t}F + \frac{\partial}{\partial \mathbf{X}} \cdot (\dot{\mathbf{X}}F) + \frac{\partial}{\partial U}(\dot{U}F) = -B_\parallel^{**}\dot{\mathbf{X}} \cdot \nabla f_0, \quad (45)$$

where the operator $\partial/\partial\mathbf{X}$ on the left side acts on the perturbed quantity only. The linearized equation for δF then becomes

$$-i(\omega - \mathbf{k} \cdot \dot{\mathbf{X}}_0)\,\delta F = -i\mathbf{k} \cdot \boldsymbol{\delta}\dot{\mathbf{X}} F_0 - \dot{U}\frac{\partial F_0}{\partial U} - (\mathbf{K} \cdot \boldsymbol{\delta}\dot{\mathbf{X}})F_0. \quad (46)$$

In Eq. (46) we have defined $\mathbf{K} = \nabla f_0/f_0$, $\dot{\mathbf{X}}_0$ and $\boldsymbol{\delta}\dot{\mathbf{X}}$ are zero- and first-order drift velocities; the perturbation is taken to be of the form $\exp(i\mathbf{k}\cdot\mathbf{x} - i\omega t)$, where $\mathbf{k} = k_\parallel\hat{\mathbf{e}}_1 + k_\perp\hat{\mathbf{e}}_2$ is the wave vector, $\hat{\mathbf{e}}_1 \equiv \hat{\mathbf{b}} = \mathbf{B}_0/B_0$ and we assume the background magnetic field and density to vary only in the $\hat{\mathbf{e}}_3$ direction, so that $\mathbf{K} = K\hat{\mathbf{e}}_3$.

Solving for δF, we obtain

$$\delta F = \left\{ iE_2\left(\frac{\omega_M(\omega-\omega^*)}{\omega - k_\parallel U - \omega_M} - \omega^*\right)\frac{J_0}{\omega k_\perp T_\parallel} + E_3\left[\frac{v_\perp J_1}{\omega T_\parallel}\left(\frac{\omega-\omega^*}{\omega - k_\parallel U - \omega_M} - 1\right) + \frac{k_\perp J_0}{\omega B_0}\right]\right\} F_0, \tag{47}$$

where we have used linearized Eqs. (9) and (10), Faraday's law, and $\nabla\cdot\boldsymbol{\delta}\mathbf{B} = 0$, and have defined

$$\begin{aligned}\omega_M &= \mathbf{k}\cdot\hat{\mathbf{b}}\times\nabla B_0\mu/B_0,\\ \omega^* &= \omega_M + \mathbf{k}\cdot\hat{\mathbf{b}}\times\mathbf{K}T_\parallel/B_0.\end{aligned} \tag{48}$$

The gyroaverages were calculated using $\langle\exp(i\mathbf{k}\cdot\boldsymbol{\rho})\rangle = J_0(k_\perp\rho)$ and $\langle\mathbf{v}_\perp\cdot\mathbf{A}(\mathbf{X}+\boldsymbol{\rho})\rangle = -iv_\perp J_1(k_\perp\rho)A_3 = -v_\perp J_1 E_3/\omega$, where J_0 and J_1 are the zero- and first-order Bessel functions.

Upon recalling that $K = d\ln(F_0/B_0)/dX_3 = \kappa_n - \kappa_B$, we can rewrite ω^* as

$$\omega^* = \left[\omega_{ni}\left(1 - \frac{\kappa_B}{\kappa_n}(1-\mu/\overline{\mu})\right) + \omega_M\left(\frac{T_\perp}{T_\parallel} - 1\right)\right]\frac{T_\parallel}{T_\perp}, \tag{49}$$

where ω_{ni} is diamagnetic drift frequency.

Only the perpendicular component of the perturbed current appears in the linearized momentum equation (1):

$$-i\omega\rho_b\mathbf{v}_b = (\boldsymbol{\delta}\mathbf{j} - \boldsymbol{\delta}\mathbf{j}_h)\times\mathbf{B}_0 - n_{h0}\mathbf{E}. \tag{50}$$

Thus we only need to calculate $\boldsymbol{\delta}\mathbf{j}_{h\perp}$

$$\boldsymbol{\delta}\mathbf{j}_{h\perp} = \int[\boldsymbol{\delta}\dot{\mathbf{X}}_\perp F_0 + (\dot{\mathbf{X}}_{0\perp} + \mathbf{v}_\perp)\delta F + \hat{\mathbf{b}} \times\mathbf{K}\langle\mathbf{v}_\perp\cdot\mathbf{A}\rangle F_0/B_0]\delta(\mathbf{X} + \boldsymbol{\rho}_h - \mathbf{x})d^3\mathbf{X}\,dU\,d\mu\,d\theta, \tag{51}$$

where the first two terms in the square brackets are the first-order part of Eq. (13) and the third term has to be added to the expression for $\mathbf{j}_h$ when the background distribution function is not uniform. This term ensures the symmetry of the resulting dielectric tensor, which is important for obtaining the correct coupling between the shear Alfvén and compressional (fast) mode. It can also be verified by making the transformation from physical space to gyrokinetic space in the first velocity moment integral. Note that Eqs. (13) and (51) are approximations valid in the case when the hot ion drift frequencies are large compared to the frequency of the wave. The more accurate expression for current, valid for arbitrary values of κ_n and κ_B, can be calculated by coordinate transformation in the six-dimensional phase-space $(\mathbf{x}, \mathbf{v})$, using the known relations between physical and gyro-center variables [7], and is beyond the scope of this article.

Since we are using the local approximation, the spatial dependence of the terms in the square brackets in Eq. (51) is of the form $\exp(i\mathbf{k}\cdot\mathbf{X})$; thus, integrating with respect to $\mathbf{X}$ and calculating gyroaverages, we obtain

$$\boldsymbol{\delta}\mathbf{j}_{h\perp} = \int\left[\left(\boldsymbol{\delta}\dot{\mathbf{X}}_\perp + \hat{\mathbf{b}}\times\mathbf{K}\frac{1}{B_0}\langle\mathbf{v}_\perp\cdot\mathbf{A}\rangle\right)J_0F_0 + (\dot{\mathbf{X}}_{0\perp}J_0 + iv_\perp J_1\hat{\mathbf{e}}_3)\delta F\right]dU\,d\mu, \tag{52}$$

where we have used $\langle\mathbf{v}_\perp\exp(-i\mathbf{k}\cdot\boldsymbol{\rho})\rangle = iv_\perp J_1\hat{\mathbf{e}}_3$. Substituting Eq. (47) into Eq. (52) for two perpendicular components of $\boldsymbol{\delta}\mathbf{j}_{h\perp}$ we obtain

$$\begin{aligned}\delta j_{h2} &= \frac{iE_2}{\omega k_\perp^2 T_\parallel}\int\left[\frac{(\omega-\omega^*)\omega_M}{\omega - k_\parallel U - \omega_M} - \omega^*\right]\omega_M J_0^2F_0\,dU\,d\mu\\ &\quad + \frac{E_3}{\omega k_\perp T_\parallel}\int\left[\left(\frac{(\omega-\omega^*)\omega_M}{\omega - k_\parallel U - \omega_M} - \omega^*\right)v_\perp J_1J_0 + \omega k_\perp T_\parallel\frac{1}{B_0}J_0^2\right]F_0\,dU\,d\mu,\end{aligned} \tag{53}$$

$$\begin{aligned}\delta j_{h3} &= -\frac{E_2}{\omega k_\perp T_\parallel}\int\left[\left(\frac{(\omega-\omega^*)\omega_M}{\omega - k_\parallel U - \omega_M} - \omega^*\right)v_\perp J_1J_0 + \omega k_\perp T_\parallel\frac{1}{B_0}J_0^2\right]F_0\,dU\,d\mu\\ &\quad + \frac{iE_3}{\omega T_\parallel}\int\left[\frac{\omega-\omega^*}{\omega - k_\parallel U - \omega_M} + \left(\frac{T_\parallel}{T_\perp} - 1\right)\right]v_\perp^2J_1^2F_0\,dU\,d\mu,\end{aligned} \tag{54}$$

where the identity $\int v_\perp^2J_1^2F_0B_0\,d\mu/T_\perp = 2\int k_\perp v_\perp J_1J_0F_0\,d\mu$ has been used to obtain Eq. (54).

Now we can substitute Eqs. (53) and (54) into the linearized momentum equation (50) and use the MHD equations (2)–(5) to obtain the dispersion relation for the MHD-gyrokinetic system

$$(\omega^2 - k_\parallel^2v_A^2 - A_{22})(\omega^2 - k^2v_A^2 - A_{33}) = A_{32}^2, \tag{55}$$

where

$$A_{22} = \frac{B_0^2}{n_bk_\perp^2T_\parallel}\int\left[\frac{(\omega-\omega^*)\omega_M}{\omega - k_\parallel U - \omega_M} - \omega^*\right]\omega_M J_0^2F_0\,dU\,d\mu, \tag{56}$$

$$A_{32} = -\frac{B_0^2}{n_b k_\perp T_\parallel}\int\left[\left(\frac{(\omega-\omega^*)\omega_M}{\omega - k_\parallel U - \omega_M} - \omega^*\right) v_\perp J_1 J_0 - \omega k_\perp T_\parallel \frac{1}{B_0}(1-J_0^2)\right] F_0\, dU\, d\mu, \quad (57)$$

$$A_{33} = \frac{B_0^2}{n_b T_\parallel}\int\left[\frac{\omega-\omega^*}{\omega - k_\parallel U - \omega_M} + \left(\frac{T_\parallel}{T_\perp} - 1\right)\right] v_\perp^2 J_1^2 F_0\, dU\, d\mu, \quad (58)$$

and $v_A^2 = B_0^2/4\pi\rho_b$ is the Alfvén speed of the bulk plasma.

In the limit of small A_{32}, such as when $\kappa_B = \kappa_n = 0$ and $k_\perp \rho_h \ll 1$, Eq. (55) describes decoupled pure transverse Alfvén and compressional waves. When the hot ion pressure and background magnetic field are nonuniform, there is significant coupling between the Alfvén and fast modes.

The coupled shear Alfvén and compressional waves in a two-component plasma (hot and cold) in slab geometry were considered, for example, in [22], where the effect of ∇B_0 and ∇n_0 on the mode coupling was studied for the high-beta case $\beta \sim 1$ and $E_\parallel = 0$. The dispersion relation obtained by Ng and Patel [22] using a kinetic description for hot particles is similar to Eq. (55), if one assumes that the plasma consists of cold electrons, cold ions, and hot ions, and sets $\nabla T_\perp/T_\perp = \nabla B_0/B_0$.

The detailed comparison of Eqs. (55)–(58) with kinetic theory results shows that the MHD-gyrokinetic model accurately describes fast magnetosonic waves, assuming that ordering (8) holds. The coupling terms, namely the off-diagonal elements of the dielectric tensor $\sim A_{32}$, are identical to those in Eq. (6) in [22], except for the term $\sim I_1 \exp(-k_\perp^2\rho_h^2/2)$, which can be neglected when the Alfvén and fast modes are coupled through the hot ion pressure gradient ($\omega^* \gg \omega(k_\perp\rho_h)^2$ in Eq. (57)). In a homogeneous plasma the coupling between the modes is due to the finite Larmor radius and it is qualitatively correctly described by Eq. (57) for $k_\perp^2\rho_h^2 \lesssim 1$. In the Alfvén wave dispersion relation only terms quadratic in the drift frequency are present. It lacks, therefore, terms of order $O(\omega/\omega^*)$ and $O(\omega^2/\omega^{*2})$, and is valid in the limit ω^*, $\omega_M \gg \omega$. The anistropy related term $\sim k_\parallel^2(T_\perp - T_\parallel)$ [22] is also missing in our expression for A_{22}. Thus the model is suitable for studying compressional type modes, in particular drift-mirror and drift-compressional instabilities. It can also be used to study pressure gradient driven instabilities of the shear Alfvén wave, provided that the drift frequency is large compared to the wave frequency and the plasma is isotropic. The dispersion equation (55) was solved numerically to calculate the linear wave frequency and growth rate, which were then compared with simulation results.

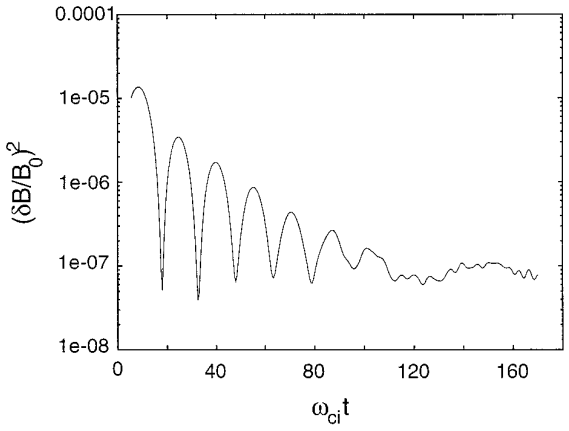

FIG. 1. The 2D hybrid MHD-gyrokinetic simulation of Landau damping of a compressional mode using 160,000 particles on a 32×32 grid and $\Delta t = 0.5$. Shown is the time history of the perturbed magnetic field energy $(\delta B/B_0)^2$.

7. SIMULATION RESULTS

The described hybrid MHD-gyrokinetic simulation scheme has been implemented in a 2D code using slab geometry. Periodic boundary conditions for fields and particles are used in both directions. The equilibrium magnetic field is assumed to be in the plane of the simulation. Since the computational time required for particle pushing greatly exceeds the time needed to solve the field equations, subcycling is used to update the fields with a small enough time step to avoid numerical instability. The particle coordinates and weight factors are advanced with a larger time step, which in this case is limited by the accuracy requirement of the small parallel displacement of the particle.

Three cases are considered. First, to benchmark the code the damping of a fast magnetosonic wave in a uniform isotropic plasma through magnetic Landau resonance with energetic ions was simulated. Two-dimensional simulations of the mirror instability driven by the hot ion temperature anisotropy were also performed. In both cases the simulation results were compared with kinetic theory results obtained using the linear dispersion relation solver WHAMP [23]. A 2D numerical model with fixed background inhomogeneity was developed using the multiple scale expansion method and it was used to study the temperature gradient-driven instability of a compressional mode for $\beta = 0.5$.

7.1. *Landau Damping of Compressional Mode*

Figure 1 shows damping of a compressional type perturbation with initial bulk velocity amplitude $v_b = 0.01 v_A$ and parallel and perpendicular wave numbers $k_\parallel\rho_h = 0.2$ and $k_\perp\rho_h = 0.4$. The parameters of the hot plasma are $v_{th\parallel} =$

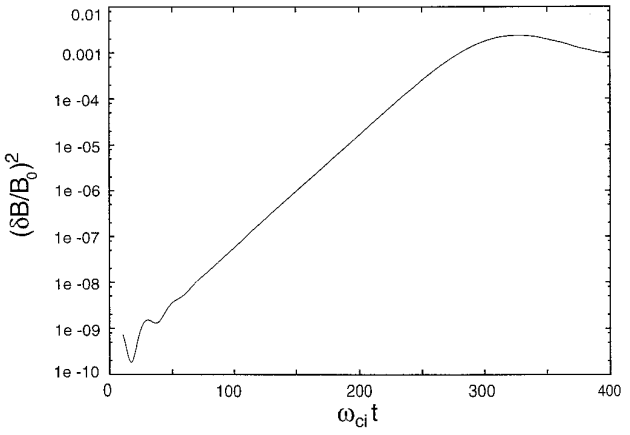

FIG. 2. The perturbed magnetic field energy as a function of time for the 2D simulation of the mirror instability with $T_\perp/T_\parallel = 2.25$, $\beta_{h\parallel} = 1.$, $n_h/n_b = 0.1$, for a run with 320,000 particles on a 64×64 grid with $\Delta t = 0.5$. Other parameters are given in the text.

$v_{th\perp} = 3.16$ and $n_h = 0.1n_b$. The bulk plasma temperature was set to be zero. In this section all velocities are normalized to the bulk Alfvén velocity v_A, time is in terms of inverse ion cyclotron frequency, and length is measured in units of v_A/ω_{ci}. The calculation employs 160,000 macroparticles randomly initialized on a 32×32 grid with grid spacing $\Delta x_\parallel = 3.125$ and $\Delta x_\perp = 1.56$. The particle time step is $\Delta t = 0.5$, with a smaller time step for field subcycling $\Delta t_f = \Delta t/4$.

Figure 1 shows that the wave field energy decreases by two orders of magnitude to the noise level at $t \approx 100$. The wave energy is absorbed by those resonant particles which have parallel velocity comparable to the wave phase velocity $U \sim \omega/k_\parallel$. The measured real frequency and damping rate are $(\omega, \gamma) = (0.2, -0.023)\omega_{ci}$, whereas kinetic theory predicts $(\omega, \gamma) = (0.2, -0.030)\omega_{ci}$. The agreement is very good considering the relatively small number of particles used in the two-dimensional simulation of high-β ($\beta = 1.0$) plasma. The total energy was conserved within 2.5% of the initial perturbation energy and the number of particles was conserved with an accuracy $\delta N/N \sim 10^{-5}$.

7.2. *Mirror Instability*

The simulation of the mirror instability was performed for the hot ion temperature anisotropy $T_\perp/T_\parallel = 2.25$ and $\beta_\parallel = 1$. The simulation was carried out using 320,000 macroparticles on a 64×64 grid with grid spacing $\Delta x_\parallel = 1.56$ and $\Delta x_\perp = 0.78$. Figure 2 shows time evolution of the perturbed magnetic field energy for the hot ion parameters: $v_{th\parallel} = 3.16$, $v_{th\perp} = 4.74$ and $n_h = 0.1n_b$. Time steps $\Delta t = 0.5$ and $\Delta t_f = 0.125$ were used for particles and fields, respectively. The instability grows from the small amplitude initial perturbation with $k_\parallel \rho_h = 0.3$ and $k_\perp \rho_h = 0.6$. The length of the system in the parallel and perpendicular directions was set to be equal to the parallel and perpendicular wavelengths of the growing mode, which is also the most unstable mode in the system. Fourier analysis shows that this mode remains dominant throughout the simulation and, therefore, its linear growth rate can be estimated from the increase in $(\delta B/B_0)^2$ as $\gamma \approx 0.029\omega_{ci}$. This is in good agreement with the linear kinetic theory result $\gamma = 0.026\omega_{ci}$.

Figure 3 shows time histories of (a) perturbed magnetic field energy, (b) hot ion kinetic energy, (c) change in the hot ion parallel (solid line) and perpendicular (dashed line) kinetic energy, and (d) averaged particle weight $\delta N/N = \sum d_m/M$, obtained in the same run as Fig. 2. All the energies are normalized to the background magnetic field energy. Since no longer wavelength modes are allowed to grow and the amplitude of the shorter wavelength modes remains small, this is essentially a one-mode regime, and Figs. 3a and b indeed exhibit the characteristic behavior of a monochromatic wave with regular nonlinear oscillations following the linear growth phase.

As the fluctuations grow, the particle parallel kinetic energy increases and the perpendicular kinetic energy decreases (Fig. 3c), thus reducing the initial temperature anisotropy. However, the instability saturates at a rather low level, $(\delta B/B_0)^2 \approx 0.002$, without a significant change in the temperature ratio. Interestingly, when the simulation was run with a larger system size, the saturation of the most

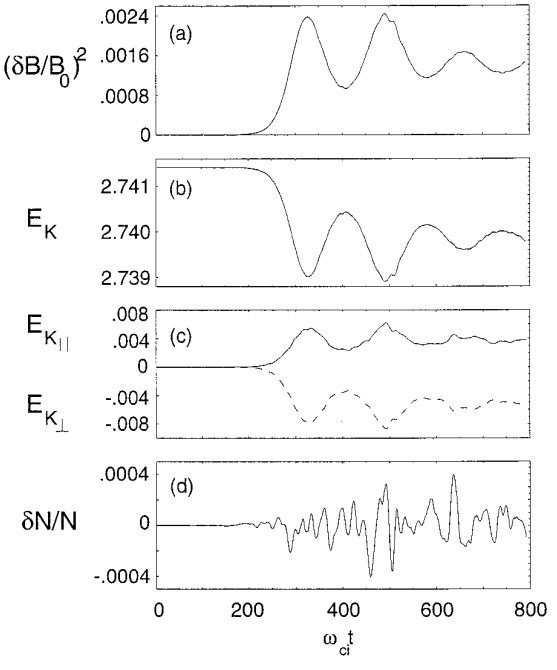

FIG. 3. Time histories of (a) $(\delta B/B_0)^2$, (b) hot ion kinetic energy, (c) change in hot ion parallel (solid line) and perpendicular (dashed line) kinetic energy, and (d) relative change in particle number $\delta N/N$, for the same simulation as Fig. 2.

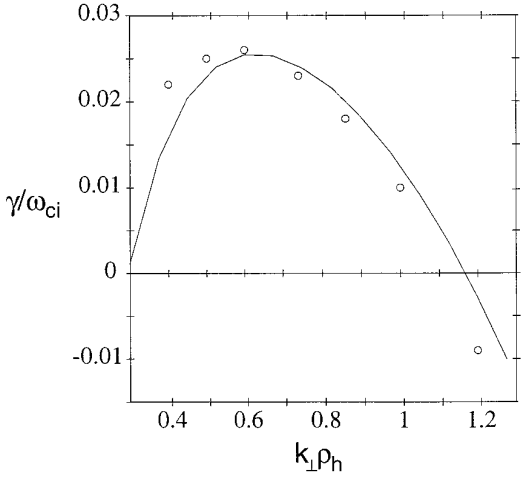

FIG. 4. The linear growth rate of the mirror instability as a function of perpendicular wave number for $T_\perp/T_\parallel = 2.25$, $\beta_{h\parallel} = 1.$, $n_h/n_b = 0.1$, and $k_\parallel\rho_h = 0.3$. The solid line is a result obtained using the dispersion relation solver WHAMP [23], the dots represent the simulation results for the runs with 40,000 particles on a 32×32 grid with $\Delta t = 0.5$.

unstable mode was succeeded by the growth of a longer wavelength mode, with higher saturation amplitude, leading to the considerable reduction of the temperature anisotrophy. The growth of longer wavelength modes was also observed in simulations of mirror modes by McKean *et al.* [24].

There was good conservation of total energy and number of particles in the simulation, with the change in total energy less than 7% of the wave energy, and $\delta N/N \sim 10^{-4}$. Since the bulk plasma pressure was zero, the change in bulk parallel momentum was negligible, while the hot ion parallel momentum was conserved, oscillating around zero value with amplitude smaller than 10^{-4}. For the set of parameters used in the simulations, conservation properties and linear growth rate are affected mostly by the size of the particle time step, which should be smaller than $\Delta x_\parallel/v_{th\parallel}$. The correct growth rate and good conservation of energy, particle number, and parallel momentum were also obtained in the simulations with a smaller number of particles, $M = 40{,}000$ and a 32×32 grid. However, a larger number of particles and finer spatial resolution were required to achieve convergence in the nonlinear behavior after saturation.

In order to investigate how well finite Larmor radius effects are reproduced by the model, simulations were performed to study the dependence of the linear growth rate of the mirror mode on $k_\perp\rho_h$. Simulations were carried out using 40,000 macroparticles on a 32×32 grid for $0.4 \le k_\perp\rho_h \le 1.2$ and the rest of the parameters are the same as in the previous case. The results are shown in Fig. 4, where the solid line represents a theoretical result, and the dots show the values of γ/ω_{ci} obtained in the simulations. The agreement is very good, except for smaller values of $k_\perp\rho_h$, for which the gyrokinetic condition $k_\parallel \ll k_\perp$ is violated.

7.3. *Drift Instability of Compressional Mode*

Simulations of the temperature gradient-driven instability of the compressional mode [25] were performed for the hot ion distribution $F_0 = n_{h0} f_M(U) \exp(-\mu/\overline{\mu})$, which corresponds to a distribution of adiabatically injected particles [13]. A background magnetic field was assumed to be nonuniform, with gradient out of the plane of the simulation. The case of $\nabla n_{h0} = 0$ and magnetic field pressure gradient balanced by the gradient in the zero-order bulk plasma pressure was considered. This approach allows one to perform 2D simulations with fixed background inhomogeneity, using periodic boundary conditions, and facilitates comparison of the simulation results with the solution of the linear dispersion relation obtained in the local approximation. The dispersion relation for this case is similar to Eq. (55). For the fast mode, the coupling to the transverse Alfvén wave can be neglected and the dispersion relation can be written as

$$\omega^2 = k^2 v_A^2 + \frac{1}{n_b}\frac{2}{\rho_h^2}\int\left(\frac{\omega - \omega_M}{\omega - k_\parallel U - \omega_M}\right) v_\perp^2 J_1^2 F_0\, dU\, d\mu, \quad (59)$$

where ω_M is magnetic drift frequency defined by Eq. (48), $T_\perp/T_\parallel = 1$ and $\nabla T_\perp/T_\perp = \nabla B_0/B_0$. The resonant ions, for which $\omega - k_\parallel U - \omega_M = 0$, will drive the instability via inverse Landau damping, if the condition $\omega < \omega_M$ is satisfied.

The simulations were carried out with $\beta_h = 0.5$, $n_h = 0.005 n_b$, and $\rho_h/L_B = 0.2$, where $L_B = |\nabla \ln B_0|^{-1}$ and $\rho_h = 10$. The wavevector of the initial perturbation was $k_\perp\rho_h = 0.8$ and $k_\parallel\rho_h = 0.2$, which corresponds to the most unstable solution of Eq. (59). The number of particles used in the simulation was 40,000 on a 16×32 grid with $\Delta x_\parallel = 18.0$ and $\Delta x_\perp = 2.5$. The particle and field time steps were $\Delta t = 1.0$ and $\Delta t_f = 0.125$.

Figure 5 shows the evolution of (a) the real part and (b) the amplitude of the compressional component of the perturbed magnetic field $\delta B_\parallel/B_0$ for the dominant Fourier mode. The growth rate measured from a logarithmic plot is $\gamma = 0.004\omega_{ci}$, and the real frequency is found to be $\omega = 0.09\omega_{ci}$, which is in very good agreement with the solution of the linear dispersion relation Eq. (59): $(\omega, \gamma) = (0.087, 0.0042)\omega_{ci}$.

The instability saturates due to resonant particle trapping by the wave. Therefore, the very small linear growth rate leads to the very low saturation level $\delta B/B_0 \approx 10.8(\gamma/k_\parallel v_{th})^2 \approx 4 \times 10^{-3}$. The estimate for the frequency of trapped particle oscillations in the wave magnetic well, $\omega_b \sim k_\parallel v_{th}\sqrt{\delta B/B_0} \approx 0.013\omega_{ci}$, agrees with the numerical

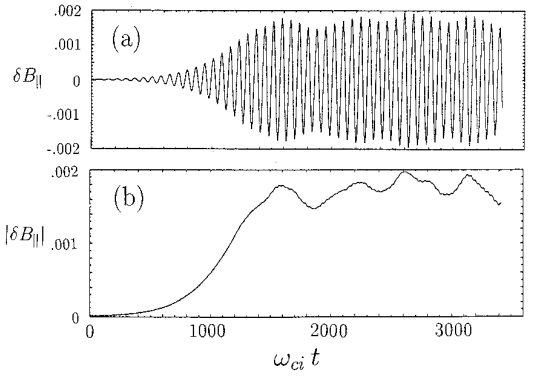

FIG. 5. The 2D simulation of drift instability of the fast mode for $\beta_h = 0.5$, $n_h/n_b = 0.005$, and $\rho_h/L_B = 0.2$: (a) The time history of the real part of the (1,1) Fourier harmonic of $\delta B_\parallel/B_0$ and (b) the corresponding amplitude evolution for a run with 40,000 particles on a 16×32 grid with $\Delta t = 1$.

result $\omega_b \sim 0.01\omega_{ci}$ (Fig. 5b). Note that the saturation amplitude of this instability is an order of magnitude lower than the thermal noise level in a conventional "full-f" code using the same parameters. Therefore, the strong reduction in the numerical noise level of the δf method allows one to perform multidimensional simulations of weak instabilities inaccessible to conventional methods.

The total energy was conserved with ~20% accuracy at $t = 1800$, although better energy conservation could be achieved using a smaller particle time step. The particle number was well conserved through the run, with $|\delta N/N| \lesssim 10^{-4}$.

Figure 6 shows a contour plot of the spatially averaged perturbed distribution function δF at $t = 1500$. The perturbation of the distribution function is largest along the lines where the resonant condition is satisfied, $\omega - k_\parallel U - \overline{\omega}_M(v_\perp/v_{th})^2 = 0$, where $\overline{\omega}_M$ is the averaged magnetic drift frequency.

8. SUMMARY

In this paper we have presented a hybrid MHD-gyrokinetic model suitable for self-consistent study of the interaction of energetic particles with low frequency MHD waves in a high-beta plasma. Based on this model a 2D hybrid code in slab geometry has been developed. The code utilizes fully electromagnetic gyrokinetic equations to advance the energetic particles and nonlinear, compressional one-fluid MHD equations are used to describe the rest of the plasma. The particles are coupled to the fluid equations using the current coupling scheme of Park *et al.* [4]. The δf method has been implemented in the code for $\beta \sim 1$ electromagnetic perturbations. The gyrokinetic description enables one to remove the restrictions on the particle time step dictated by the gyromotion, while the δf algorithm strongly reduces the numerical noise level in the simulation plasma. Therefore, considerably larger time steps and a smaller number of particles can be used in the simulations as compared to conventional methods.

To verify our hybrid MHD-gyrokinetic model, the linear dispersion relation describing the coupling between shear Alfvén and fast magnetosonic waves due to a hot ion pressure gradient and finite Larmor radius effects has been derived. The dispersion analysis shows that the model correctly describes compressional modes and coupling between the transverse and compressional perturbations. The shear Alfvén wave dispersion is accurate when drift frequencies are large compared to the frequency of the wave.

Very good agreement in terms of linear frequency and growth rate between the simulation results, kinetic theory, and solution of the derived dispersion relation was obtained. The total energy, particle number, and parallel momentum were also well conserved in the simulations.

This work is a first step in developing a numerical model suitable for studying low-frequency phenomena in a two-component plasma. It is aimed primarily at study of the self-consistent effect of magnetospheric MHD waves on energetic ring current ions, although the model has more general applications in space and laboratory plasmas.

More physics can be added to the present model; in particular, inclusion of curvature effects would allow one to study excitation of low-frequency waves in the magneto-

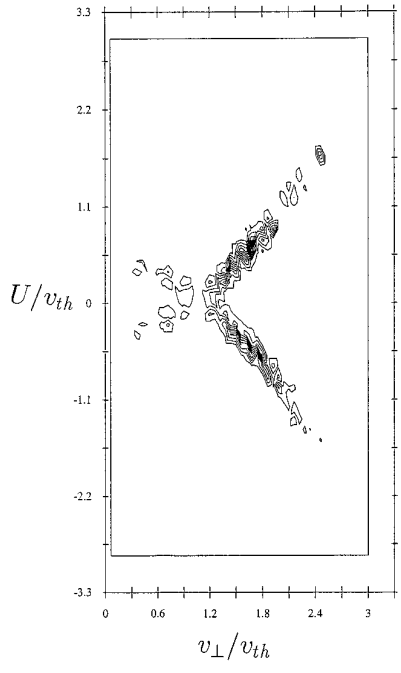

FIG. 6. Contour plots of the spatially averaged perturbed distribution function δF at $t = 1500$ from the same simulation as Fig. 5. The perturbation of the distribution function is largest along the lines where the resonant condition is satisfied: $\omega - k_\parallel U - \overline{\omega}_M(v_\perp/v_{th})^2 = 0$.

sphere using a realistic pressure balance. A more accurate expression for particle current, including the hot ion polarization current, can be used in the code and will lead to the Alfvén wave dispersion relation correct for arbitrary values of ω/ω^*. Finally, nonlinear gyro-center equations can be used in order to more accurately represent the nonlinear evolution of the MHD-gyrokinetic system.

ACKNOWLEDGMENTS

This work was supported by NSF Grants ATM-9212000, ATM-9622071 and NASA grant NAG 5-1098.

REFERENCES

1. L. Chen and A. Hasegawa, Kinetic theory of geomagnetic pulsations 1: internal excitations by energetic particles, *J. Geophys. Res.* **96,** 1503 (1991).
2. G. Y. Fu and W. Park, Nonlinear hybrid simulations of the toroidicity-induced Alfven eigenmode, *Phys. Rev. Lett.* **74,** 1594 (1995).
3. C. Z. Cheng, A kinetic-magnetohydrodynamic model for low-frequency phenomena, *J. Geophys. Res.* **96,** 21159 (1991).
4. W. Park *et al.,* Three-dimensional hybrid gyrokinetic-magnetohydrodynamic simulation, *Phys. Fluids* **4,** 2033 (1992).
5. Y. Todo *et al.,* Magnetohydrodynamic Vlasov simulations of the toroidal Alfven eigenmode, *Phys. Plasmas* **2,** 2711 (1995).
6. S. Briguglio, G. Vlad, and C. Kar, Hybrid magnetohydrodynamic-gyrokinetic simulation of toroidal Alfven modes, *Phys. Plasmas* **2,** 3711 (1995).
7. A. Brizard, Nonlinear gyrokinetic Maxwell–Vlasov equations using magnetic coordinates, *J. Plasma Phys.* **41,** 541 (1989).
8. A. A. Chan, Interaction of energetic ring current protons with magnetospheric hydromagnetic waves, Ph.D. thesis, Princeton University, 1991.
9. D. H. E. Dubin, J. A. Krommes, C. Oberman, and W. W. Lee, Nonlinear gyrokinetic equations, *Phys. Fluids* **26,** 3524 (1983).
10. T. S. Hahm, W. W. Lee, and A. Brizard, Nonlinear gyrokinetic theory for finite-beta plasmas, *Phys. Fluids* **31,** 1940 (1988).
11. M. Kotschenreuther, *Bull. Am. Phys. Soc.* **34,** 2107 (1988).
12. G. Hu and J. A. Krommes, Generalized weighting scheme for δf particle-simulation method, *Phys. Plasmas* **1,** 863 (1994).
13. D. J. Southwood, A general approach to low frequency instability in the ring current plasma, *J. Geophys. Res.* **81,** 3340 (1976).
14. W. W. Lee, Gyrokinetic particle simulation model, *J. Comput. Phys.* **72,** 234 (1987).
15. R. G. Littlejohn, Variational principles of guiding center motion, *J. Plasma Phys.* **29,** 111 (1983).
16. K. Takahashi, Multisatellite studies of ULF waves, *Adv. Space Res.* **8,** 427 (1988).
17. W. Baumjohann, N. Sckopke, J. LaBelle, B. Klecker, H. Lühr, and K. H. Glassmeier, Plasma and field observations of a compressional Pc 5 wave event, *J. Geophys. Res.* **92,** 12203 (1987).
18. S. E. Parker and W. W. Lee, A fully nonlinear characteristic method for gyrokinetic simulation, *Phys. Fluids* **5,** 77 (1993).
19. T. S. Hahm, Nonlinear gyrokinetic equations for tokamak microturbulence, *Phys. Fluids* **31,** 2670 (1988).
20. A. Y. Aydemir, A unified Monte Carlo interpretation of particle simulations and applications to non-neutral plasmas, *Phys. Plasmas* **1,** 822 (1994).
21. R. E. Denton and M. Kotschenreuther, δf Algorithm, *J. Comput. Phys.* **119,** 283 (1995).
22. P. H. Ng and V. L. Patel, The coupling of shear Alfven and compressional waves in high-β magnetospheric plasma, *J. Geophys. Res.* **88,** 10035 (1983).
23. K. Rönnmark, Computation of the electric tensor of a Maxwellian plasma, *Plasma Phys.* **25,** 669 (1983).
24. M. E. McKean, D. Winske, and S. P. Gary, Mirror and ion cyclotron anisotropy instabilities in the magnetosheath, *J. Geophys. Res.* **97,** 19421 (1992).
25. A. Hasegawa, Drift-wave instabilities of a compressional mode in a high-β plasma, *Phys. Rev. Lett.* **27,** 11 (1971).